Received: 18 October 2022 | Revised: 27 January 2023 | Accepted: 31 January 2023

DOI: 10.1111/cas.15749

Cancer Science WILEY

ORIGINAL ARTICLE

EFHD1, a novel mitochondrial regulator of tumor metastasis in clear cell renal cell carcinoma

Kun Meng[1,2] | Yuyu Hu[1] | Dingkang Wang[1] | Yuying Li[1] | Fujin Shi[1] | Jiangli Lu[3] | Yang Wang[1] | Yun Cao[3] | Chris Zhiyi Zhang[1] | Qing-Yu He[1,2]

[1]MOE Key Laboratory of Tumor Molecular Biology and Key Laboratory of Functional Protein Research of Guangdong Higher Education Institutes, Institute of Life and Health Engineering, Jinan University, Guangzhou, China

[2]The First Affiliated Hospital of Jinan University, Guangzhou, China

[3]Department of Pathology, State Key Laboratory of Oncology in South China, Sun Yat-sen University Cancer Center, Guangzhou, China

Correspondence
Chris Zhiyi Zhang, MOE Key Laboratory of Tumor Molecular Biology and Key Laboratory of Functional Protein Research of Guangdong Higher Education Institutes, Institute of Life and Health Engineering, Jinan University, Huang-Pu Avenue West 601, Guangzhou 510632, China.
Email: zhangzy@jnu.edu.cn

Qing-Yu He, MOE Key Laboratory of Tumor Molecular Biology and Key Laboratory of Functional Protein Research of Guangdong Higher Education Institutes, Institute of Life and Health Engineering, Jinan University, Huang-Pu Avenue West 601, The First Affiliated Hospital of Jinan University, Huang-Pu Avenue West 613, Guangzhou 510632, China.
Email: tqyhe@email.jnu.edu.cn

Funding information
Guangdong Basic and Applied Basic Research Foundation, Grant/Award Number: 2022A1515111106; National Key Research and Development Program of China, Grant/Award Number: 2017YFA0505100 and 2020YFE0202200; National Natural Science Foundation of China, Grant/Award Number: 31770888 and 31570828

Abstract

The biological function of many mitochondrial proteins in mechanistic detail has not been well investigated in clear cell renal cell carcinoma (ccRCC). A seven-mitochondrial-gene signature was generated by Lasso regression analysis to improve the prediction of prognosis of patients with ccRCC, using The Cancer Genome Atlas and Clinical Proteomic Tumor Analysis Consortium cohort. Among those seven genes, *EFHD1* is less studied and its role in the progression of ccRCC remains unknown. The decreased expression of EFHD1 was validated in clinical samples and was correlated with unfavorable outcome. Overexpression of EFHD1 in ccRCC cells resulted in the reduction of mitochondrial Ca^{2+}, and the inhibition of cell migration and invasion in vitro and tumor metastasis in vivo. Mechanistically, EFHD1 physically bound to the core mitochondrial calcium transporter (mitochondrial calcium uniporter, MCU) through its N-terminal domain. The interaction between EFHD1 and MCU suppressed the uptake of Ca^{2+} into mitochondria, and deactivated the Hippo/YAP signaling pathway. Further data revealed that the ectopic expression of EFHD1 upregulated STARD13 to enhance the phosphorylation of YAP protein at Ser-127. The knockdown of STARD13 or the overexpression of MCU partly abrogated the EFHD1-mediated induction of phosphorylation of YAP at Ser-127 and suppression of cell migration. Taken together, the newly identified EFHD1–MCU–STARD13 axis participates in the modulation of the Hippo/YAP pathway and serves as a novel regulator in the progression of ccRCC.

KEYWORDS
clear cell renal cell carcinoma, EFHD1, mitochondria, prognosis, tumor metastasis

Abbreviations: ccRCC, clear cell renal cell carcinoma; CPTAC, Clinical Proteomic Tumor Analysis Consortium; DIA, data-independent acquisition; EFHD1, EF-hand domain family member D1; ER, endoplasmic reticulum; MCU, mitochondrial calcium uniporter; mitoDEG, differentially expressed mitochondrial gene; mitoDEP, differentially expressed mitochondrial protein; MS, mass spectrometry; PLGEM, Power Law Global Error Model; RNA-seq, RNA sequencing; ROS, reactive oxygen species; STARD13, StAR related lipid transfer domain containing 13; TCGA, The Cancer Genome Atlas.

Kun Meng and Yuyu Hu contribute equally to this study.

1 | INTRODUCTION

The Understudied Proteins Initiative has been recently drafted by scientists from six countries to catalyze mechanistic investigations of the under-characterized proteins.[1] In cancer cells, the annotation of mitochondrial proteins remains quite limited. Clear cell renal cell carcinoma, accounting for more than 75% of kidney cancer,[2,3] takes place in kidney, the organ with mitochondrial content second only to the heart; thus, ccRCC is often considered a metabolic disease with mitochondrial dysfunction.[4,5] The 5-year survival rate of patients with metastatic ccRCC is less than 10%.[6] Therefore, exploring the dysregulation of mitochondria-related genes and their roles in the development of ccRCC may provide therapeutic strategies targeting the restoration of a steady mitochondrial state.[7–10]

EF-hand domain family member D1 is a calcium ion-regulating protein located on mitochondria.[11,12] It is involved in cell fate determination, such as osteoblast differentiation and axonal morphogenesis.[11,13] The expression of EFHD1 was evaluated by genomic studies in breast cancer and colorectal cancer,[14] but its role in tumor progression has rarely been investigated. Analyses of ccRCC data from TCGA indicated EFHD1 as a prognostic marker.[15,16] EFHD1 was regulated by HNF4 alpha in HEK293 cells.[17,18] Data of the documented studies call for a further investigation to disclose the role of EFHD1 in the malignant behavior of ccRCC.

In this study, we undertook bioinformatics analysis to screen for mitochondrial proteins associated with ccRCC prognosis. The expression of EFHD1 and its clinical implication in ccRCC was next determined. The biological function of EFHD1 and the underlying mechanism were uncovered to provide detailed annotation of EFHD1. Our study could offer a new prognostic and therapeutic biomarker to the clinical management of ccRCC.

2 | MATERIALS AND METHODS

2.1 | Bioinformatics analysis

Transcriptome and proteome data were downloaded from TCGA and CPTAC cohort. The Wilcoxon test was used to determine the statistical significance of tumor and nontumoral samples. In a univariate Cox analysis based on the standard of $p < 0.01$, the risk score of the patient was calculated by the following formula: risk score = coef (mitoDEP) × expression (mitoDEP), where coef (mitoDEP) and expression (mitoDEP) represent the survival correlation regression coefficient and expression value. coef, coefficient.

2.2 | Clinical samples and cell lines

Human ccRCC and normal renal tissues were surgically collected from ccRCC patients at Sun Yat-sen University Cancer Center. This study was approved by the institutional research ethics committee of Sun Yat-sen University Cancer Center. ACHN, 769-P, HK-2, and 293T cells were validated by short tandem repeat, and tested negative for mycoplasma. ACHN and 293T cells were cultured in DMEM (Gibco, Invitrogen), 769-P and HK-2 cells were cultured in RPMI-1640 medium (Gibco, Invitrogen); 1% penicillin–streptomycin (Gibco, Invitrogen) and 10% FBS (Gibco, Invitrogen) were added, and cells were cultured at 37°C with 5% CO_2.

2.3 | Cell transfection and lentivirus infection

Lipofectamine 3000 (Gibco, Invitrogen) was used for the transfection experiment according to the manufacturer's instructions. The sequences of siRNA are listed in Table S1. The 293T cells were transfected with pLVX-EFHD1 together with psPAX2 and pMD2.G lentiviral packaging systems (Addgene) to generate EFHD1 stably overexpressed cell lines.

2.4 | Transwell assay

Transwell chambers coated with or without Matrigel (BD Biosciences) were used to test the migration or invasion of ccRCC. Cells in FBS-free medium were seeded into the upper chamber, and 600 μl FBS-containing medium was added to the bottom chamber of the Transwell. Cells that had migrated into the lower chamber of the Transwell were fixed with methanol and stained with crystal violet (Sigma-Aldrich).

2.5 | Wound healing

Cells were seeded into 6-well tissue culture plates until they reached approximately 95% confluence as a monolayer. Parallel scratches were made gently and slowly in the monolayer in each well using a new pipette tip. After gentle washing with PBS twice, all wells were refilled with fresh serum-free medium and photographed. Following 12 h of incubation, all the wells were photographed in the same field.

2.6 | Western blot analysis

Cells were lysed in lysis buffer (Cell Signaling Technology), the BCA Kit (Thermo Fisher Scientific) was used to quantify the protein, SDS-PAGE was used to separate proteins, a PVDF membrane (Millipore) with a pore size of 0.22 μM was used to transfer, and 5% nonfat milk as a blocking agent for 1 h at room temperature. The following primary Abs were used: EFHD1 (H00080303-M05; Abnova, 1:1000), β-actin (AC038; Abclonal, 1:5000), YAP (13584-1-AP; Proteintech, 1:4000), pYAP(S127) (T55743; Abmart, 1:1000), HA (M20003; Abmart, 1:1000), Flag (20543-1-AP; Proteintech, 1:5000), MCU (26312-1-AP; Proteintech, 1:1000). Horseradish

peroxidase-linked goat anti-rabbit/mouse IgG was used as the secondary Ab.

2.7 | Immunohistochemistry assays

Paraffin tissue sections were deparaffinized, dehydrated, antigen-retrieved, and underwent nonspecific binding blockade. The sections incubated with primary Abs against EFHD1 (Abnova) overnight at 4°C. Subsequently, the sections were washed with TBS, treated with 3% H_2O_2 to block endogenous peroxidase activity, and incubated with HRP-conjugated secondary Ab and DAB substrates for staining. The percentage of positive cells were scored as: 1, <25%; 2, 25%–50%; 3, 50%–75%; 4, >75%. The intensity of staining was scored as: 0, negative; 1, weak; 2, moderate; 3, strong. Total score = positive percentage × intensity.

2.8 | Coimmunoprecipitation experiment

Western and IP lysis solutions (Beyotime) were used to dissolve cells. Immunoglobulin G or primary Abs were added for immunoprecipitation at 4°C overnight. Protein A/G Plus-Agarose (Santa Cruz Biotechnology) was added to each sample tube and immunoprecipitated at 4°C for 4 h. Western and IP lysis buffer was used to wash Protein A/G Plus-Agarose five times before western blot analysis.

2.9 | Mass spectrometry and bioinformatics analyses

Data-independent acquisition MS was used for proteins identification as we have previously described.[19] In brief, samples were dissolved in 2% SDS lysis buffer and tryptic digestion through the FASP method. Proteome Discover (Thermo Fisher Scientific) and Spectronaut (Biognosys) software was used to quantify.

2.10 | RNA sequencing

The RNA-seq was carried out by LC Sciences. Gene profiles in two conditions were analyzed by the DESeq R package (4.0.3). The genes with $p < 0.05$ and fold change more than 2 determined by EdgeR were represented as differentially expressed RNAs.

2.11 | Mitochondrial calcium detection

Rhod-2 AM (Abcam) was added to cell medium at 37°C for 40 min. Cells were washed three times with PBS, then incubated at 37°C for 40 min to complete hydrolysis. Mitochondrial Ca^{2+} was monitored by fluorescence microscope (Nikon). Thapsigargin was added to stimulate Ca^{2+} release from ER under stress, and real-time mitochondrial Ca^{2+} levels were monitored.

2.12 | Immunofluorescence assays

Cells were fixed with 4% paraformaldehyde and permeabilized by 0.1% Triton X-100, and 5% BSA was used for blocking for 1 h at room temperature. Primary Ab was incubated overnight at 4°C, then washed with TBST three times. The fluorescent secondary Ab was incubated at room temperature for 1 h; DAPI was used to stain nucleus.

2.13 | Animal experiments

Four-week-old NCG mice (stock no. T001475) were purchased from GemPharmatech, and animal experiments were constructed as described before.[20] One million cells stably expressing luciferase with EFHD1 or control ACHN cells were used per mouse. Cells were injected through the tail vein of mice for 5 weeks. Metastasis cells were monitored by bioluminescent imaging (IVIS Lumina Series III preclinical in vivo imaging system; PerkinElmer). At the end of the experiment, the lungs were dissected and examined histologically for presence of metastasis.

2.14 | Nucleus and cytoplasm separation

Solution A (500 µl; 10 mM Tris, 10 mM KCl, 5 mM MgCl, pH 7.6) was used to homogenize one million cells. Solution B (500 µl; 10 mM Tris, 10 mM KCl, 5 mM MgCl, 0.6% Triton X-100, pH 7.6) was added and lysed on ice for 30 min. Then 500 µl solution C (10 mM Tris, 10 mM KCl, 5 mM MgCl, 0.35 M source, pH 7.6) was added to the mixture. After centrifugation at 600 *g* for 10 min, the pellet is the nucleus. The supernatant was transferred and centrifuged at 10,000 *g* for 30 min at 4°C, and cytoplasmic proteins were dissolved in the supernatant.

2.15 | Statistical analysis

All the key experiments' data from at least three times are expressed as mean ± SD. We applied GraphPad Prism 7.0 software for statistical analysis and illustration. Student's *t*-test was used to analyze differences between the two groups. Experimental data were considered to represent a significant difference only if $p < 0.05$.

3 | RESULTS

3.1 | Seven-mitochondrial-gene signature to predict the prognosis of patients with ccRCC

To understand the alteration of essential signaling pathways in ccRCC, we used Gene Set Enrichment Analysis, using proteome data from CPTAC. We found that mitochondrial function was significantly inhibited in ccRCC (Figure 1A). A total of 2124 mitochondrial function-related genes confirmed in three datasets were selected

for further analyses (Figure S1A). Differentially expressed mitochondrial genes ($p < 0.05$ and |fold change| > 1.5) and mitoDEPs ($p < 0.05$ and |fold change| > 1.2) were identified in TCGA and CPTAC cohorts (Figure S1B). A panel consisting of 30 differentially expressed mitochondrial proteins that were of the same alteration trends at both RNA and protein levels was constructed (Figure 1B) and was shown by the heatmap (Figure 1C). To explore the prognostic value of the 30 MitoDEPs in ccRCC, we carried out univariate COX proportional hazards regression analysis. Results showed that 19 MitoDEPs were significantly associated with ccRCC survival (Figure 1D). LASSO Cox analysis was further carried out to test the independencies (Figure 1E). Seven MitoDEPs (ADH5, DEPTOR, SHC1, SYNE2, EFDH1, BPNT1, and BTD) with independent prognostic value in ccRCC were finally chosen for the establishment of a gene signature to predict the clinical outcome of ccRCC patients (Figure 1F). The expression of these proteins were abbreviated as exp, and the risk score calculated by the following formula: Risk score = (−1.04 * ADH5 exp.) + (−0.13 * DEPTOR exp.) + (1.07 * SHC1 exp.) + (−0.18 * EFDH1 exp.) + (−0.68 * SYNE2 exp.) + (−0.36 * BPNT1 exp.) + (−0.38 * BTD exp.) (Figure 1G).

To evaluate the reliability and sensitivity of the prognostic risk-related signature, we randomly divided the ccRCC patients into training and testing groups (Figure 1H). According to the median risk score, patients were divided into high- and low-risk groups. Kaplan–Meier survival analyses were further undertaken, and we found that patients with high-risk score were accompanied with shorter survival time in both training and testing groups (Figure 1I). The expression of mitoDEPs is illustrated by heatmaps (Figure 1J). Higher mortality was observed in patients with high-risk scores (Figure 1K). The prognostic model achieved good predictive performance in both groups, as the area under the curve values of 1-, 2-, and 3-year survival reached approximately 0.7 (Figure S1C,D). Furthermore, the association between mitoDEP signatures and clinicopathologic characteristics was determined. Results showed that patients with high-risk scores were likely to have higher pathological grade and advanced clinical TNM stages (Figure 1L). Taken together, a seven-mitochondrial-gene signature that is of prognostic value was generated.

3.2 | Expression of EFHD1 is decreased in ccRCC and correlated to poor outcomes

EFHD1, *SHC1*, and *DEPTOR*, but not the other four genes in the signature, have been documented in renal cell carcinoma. Furthermore, *EFHD1* is mostly dysregulated and its biological function has been barely known in ccRCC. Therefore, we next intended to investigate the expression and the role of *EFHD1* in ccRCC. Expression of EFHD1 in ccRCC tissues was significantly downregulated at the mRNA level in the TCGA cohort (Figure 2A) and at the protein level in the CPTAC cohort (Figure 2B), compared to the adjacent nontumoral tissues. Decreased expression of EFHD1 was correlated to high pathological grades and advanced stages (Figure 2C,D). The ccRCC patients with more EFHD1 had better overall survival (Figure 2E). Western blot analysis was used to detect the expression of EFHD1 in HK-2 human renal proximal tubule cells and ACHN and 769-P ccRCC cells. As shown in Figure 2F, EFHD1 expression was reduced in ccRCC cell lines compared to the HK-2. Furthermore, we detected the EFHD1 expression in seven paired fresh paracancerous and ccRCC samples. Results showed that the protein level of EFHD1 in the paracancerous tissue was noticeably higher than in the tumor tissue (Figure 2G). Immunohistochemistry assays were carried out to compare the expression of EFHD1 in 43 pairs of ccRCC and adjacent nontumoral tissues. The results showed that EFHD1 expression was significantly downregulated in ccRCC tissues (Figure 2H). Collectively, EFHD1 expression is decreased in ccRCC and significantly correlates with poor prognosis, suggesting that EFHD1 might participate in the progression of ccRCC.

3.3 | EFHD1 is a tumor suppressor in ccRCC

We constructed stably expressed EFHD1 ACHN and 769-P cell lines by lentiviral infection (Figure 3A). As EFHD1 has been identified as a Ca^{2+} sensor in mitochondria, we firstly explored whether EFHD1 was able to modulate the mitochondrial Ca^{2+} level. Using Rhod-2 AM staining, we found that intracellular mitochondrial

FIGURE 1 A seven-mitochondrial-gene signature was generated to predict the prognosis of patients with clear cell renal cell carcinoma (ccRCC). (A) Gene Set Enrichment Analysis shows that mitochondrial functions were significantly inhibited in ccRCC samples compared with normal samples by the Clinical Proteomic Tumor Analysis Consortium (CPTAC) cohort. (B) Thirty differentially expressed mitochondrial proteins (mitoDEPs) that showed the same alteration trends at both RNA and protein levels in The Cancer Genome Atlas (TCGA) and CPTAC cohorts. The Wilcoxon test was used to determine statistical significance. (C) Heatmap shows the expression of differentially expressed mitochondrial genes (mitoDEGs) in the TCGA cohort and mitoDEPs in the CPTAC cohort. N, nontumor; T, tumor. (D) Univariate Cox regression analysis of 19 differentially expressed prognostic signatures. Among them, 13 mitoDEPs were protective factors (hazard ratio [HR] <1, $p < 0.05$), whereas 6 of them were high-risk factors (HR >1, $p < 0.05$). (E–G) Identification of 7 mitoDEPs prognostic signatures using Lasso regression. (E) Lasso regression for the 19 mitochondrial prognostic genes, (F) cross-validation for tuning the parameter selection in the Lasso regression, and (G) coefficient of each mitoDEP in the prognostic signatures. (H) Distribution of patients in the training set and testing set. ccRCC patients were randomly divided into training and testing groups, high and low risk were divided by median risk score. (I) Kaplan–Meier curves for comparing the overall survival in training and testing sets ($p < 0.001$, log–rank test). (J) Heatmap shows the connections between expression profiles of the signature features and the risk groups in training and testing groups. (K) Survival status for each patient in the training groups and testing groups. Low-risk population: on the left side of the dotted line; high-risk population: on the right side of the dotted line. (L). Heatmap for the connections between clinicopathologic characteristics and the clusters of risk. From blue to red means increased gene expression. $^{*}p < 0.05$, $^{**}p < 0.01$, $^{***}p < 0.001$ (χ^2-test).

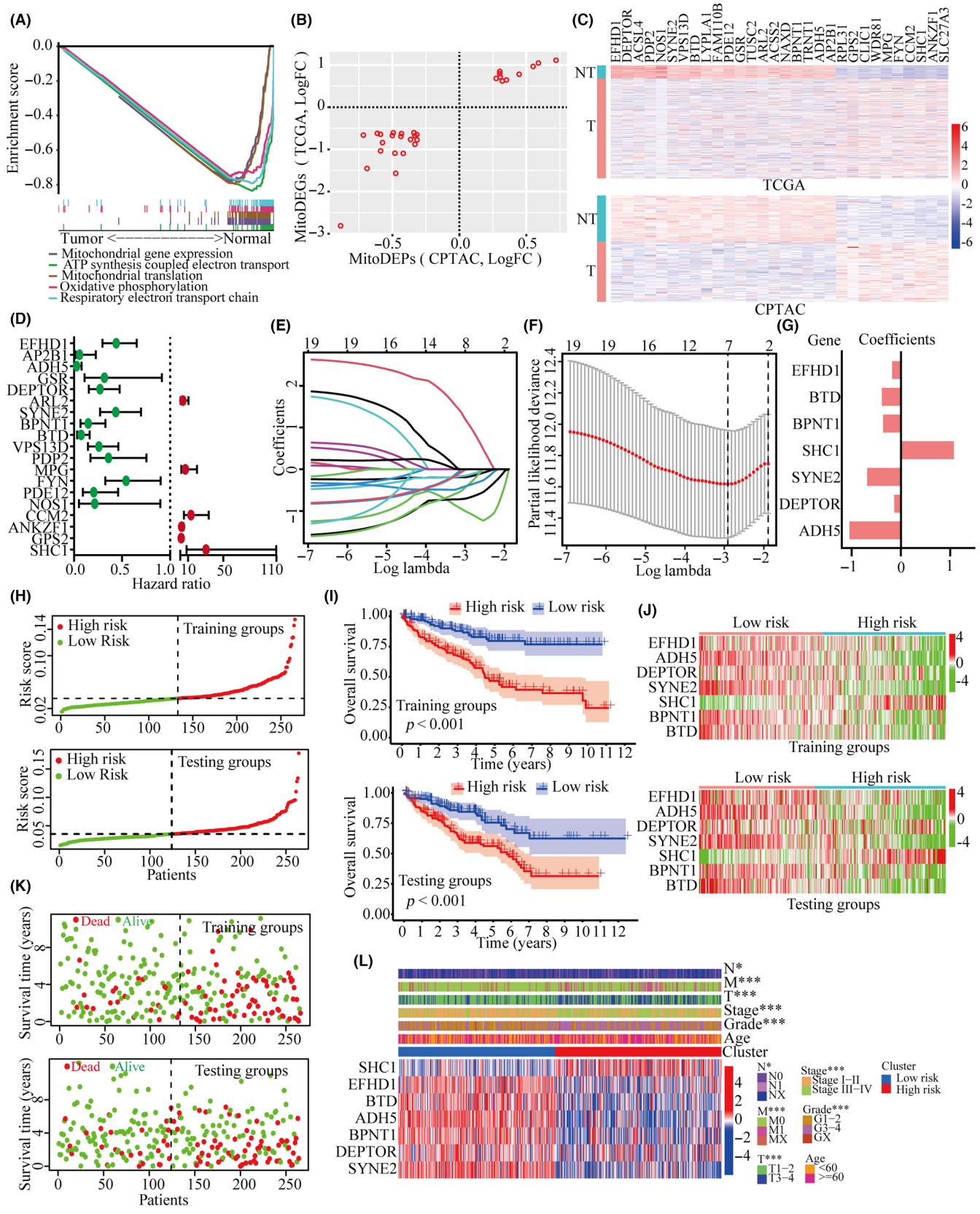

Ca^{2+} was significantly reduced upon the overexpression of EFHD1 (Figure 3B). Reactive oxygen species levels were also inhibited by EFHD1-overexpressed ccRCC cells (Figure S2A,B). We next tested the effect of EFHD1 overexpression on the uptake of mitochondrial Ca^{2+}, thapsigargin was used to stimulate the release of ER Ca^{2+} to trigger the uptake of mitochondrial Ca^{2+} through the ER–mitochondrial microregion. Thapsigargin stimulation of ACHN and 769-P cells and real-time changes of mitochondrial Ca^{2+} levels were monitored. As

shown in Figure 3C, the mitochondrial Ca^{2+} uptake capacity was significantly reduced in cells with ectopic expression of EFHD1.

Clinically, the expression of EFHD1 was significantly decreased in metastatic ccRCC patients (Figure 3D). Overexpression of EFHD1 was not capable of affecting ccRCC cell proliferation (Figure S3A,B). We next determined the role of EFHD1 in cell migration. Overexpression of EFHD1 markedly inhibited the migration and invasion of ccRCC cells (Figure 3E). Wound healing assays were

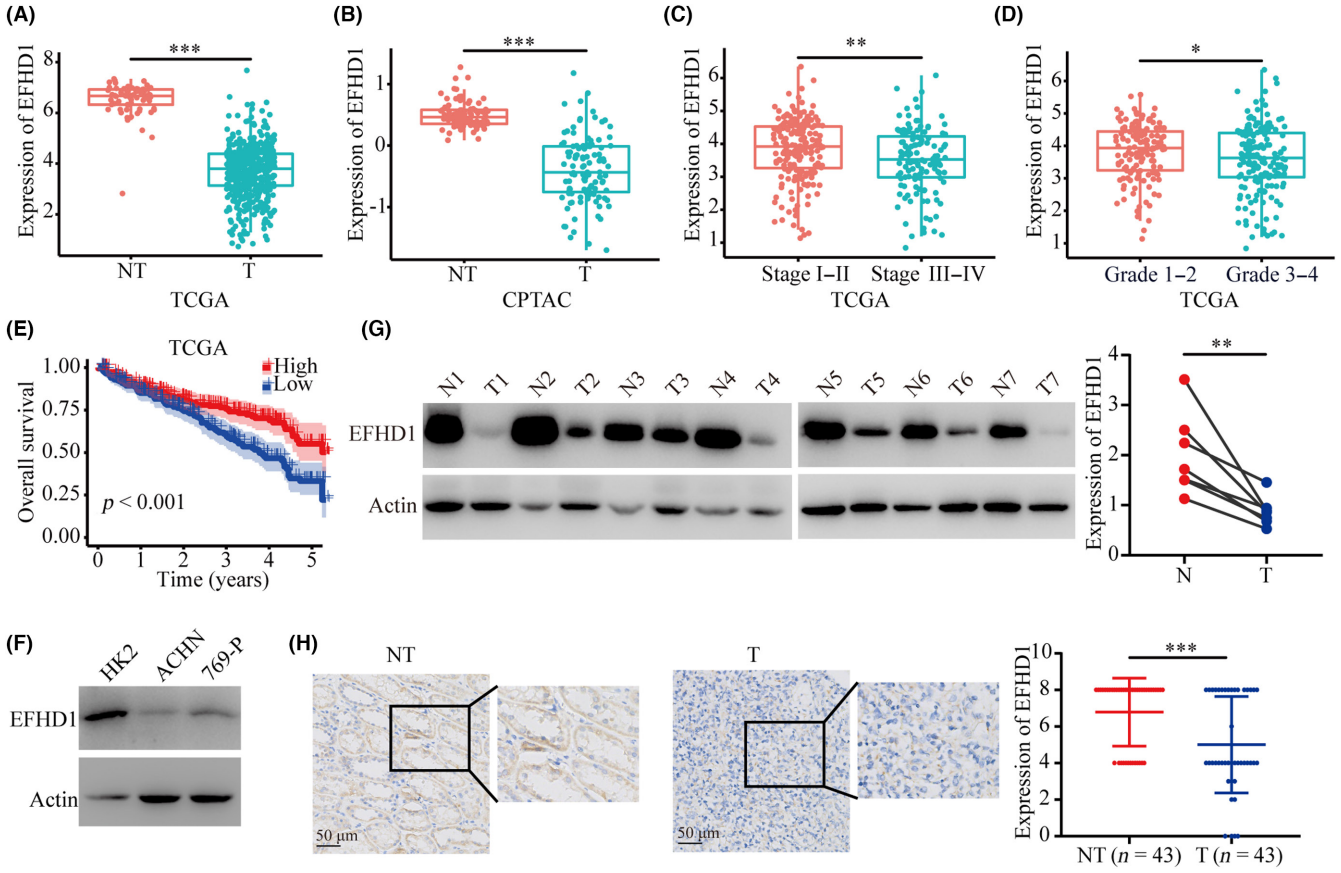

FIGURE 2 EFHD1 expression is decreased in clear cell renal cell carcinoma (ccRCC) and is correlated to poor outcomes. (A,B) Comparisons of EFHD1 expression in ccRCC tissue (T) and nontumoral tissue (NT) from (A) The Cancer Genome Atlas (TCGA) and (B) Clinical Proteomic Tumor Analysis Consortium (CPTAC) cohorts. ***$p < 0.001$ (Wilcoxon test). (C) EFHD1 expression was lower in patients with higher ccRCC stages from the TCGA cohort. **$p < 0.01$ (Wilcoxon test). (D) EFHD1 expression was lower in patients with higher ccRCC grades from the TCGA cohort. *$p < 0.05$ (Wilcoxon test). (E) ccRCC patients with high expression of EFHD1 had a better prognosis. (F) EFHD1 is highly expressed in HK-2 normal kidney cells compared with ccRCC cells. (G) EFHD1 was detected in the indicated cancer tissues (T) and their corresponding adjacent nontumoral tissues (N). **$p < 0.01$ (Student's *t*-test). (H) Representative immunohistochemistry images of EFHD1 expression in ccRCC tissues and their corresponding NT tissues. Statistics showed EFHD1 expression scores between ccRCC tissues (T) and the corresponding nontumoral tissues (NT). ***$p < 0.001$ (Student's *t*-test).

FIGURE 3 EFHD1 is a tumor suppressor in clear cell renal cell carcinoma (ccRCC). (A) Western blotting confirmed EFHD1 was overexpressed in AHCN and 769-P cells. (B) Immunofluorescence showed that overexpression of EFHD1 reduced mitochondrial Ca^{2+} concentrations. Ca^{2+} was indicated by Rhod-2 AM (red), mitochondria stained with mito-tracker (green). (C) Mitochondrial Ca^{2+} uptake capacity was inhibited after overexpression of EFHD1. Thapsigargin (TG) stimulated and monitored the change of mitochondrial Ca^{2+} concentration in real-time and performed statistics. (D) EFHD1 expression was lower in metastatic ccRCC patients from The Cancer Genome Atlas (TCGA) cohort. ***$p < 0.001$ (Wilcoxon test). (E) ACHN and 769-P cells were transfected with EFHD1, and migration and invasion abilities were determined by Transwell assays. Data are presented as mean ± SD. $n = 3$, **$p < 0.01$, ***$p < 0.001$ (Student's *t*-test). Scale bar, 300 μm. (F) ACHN and 769-P cells were transfected with EFHD1 and wound healing abilities were determined. Scale bar, 100 μm. (G) ACHN and 769-P cells were transfected with EFHD1, and less intense F-actin polymerization (red) was detected by immunofluorescence. Nuclei were stained with DAPI (blue). (H) Western blotting confirmed EFHD1 was silenced in AHCN and 769-P cells. (I) ACHN and 769-P cells were transfected with the indicated siRNA, and migration and invasion abilities were determined using Transwell assays. *$p < 0.05$, **$p < 0.01$, ***$p < 0.001$ (Students *t*-test). Scale bar, 300 μm. (J) NCG mice were transplanted with EFHD1-overexpression and luciferase-labeled ACHN cells (1×10^6 cells/mouse) through tail vein injection. Luciferase activity was visualized 5 weeks post-transplantation. *$p < 0.05$ (Student's *t*-test). (K) Histological analysis of pulmonary metastases in the mouse model was carried out using H&E staining. **$p < 0.01$ (Student's *t*-test).

carried out to confirm the inhibitory effect of EFHD1 on cell motility (Figure 3F). Moreover, immunofluorescence staining showed less intense F-actin polymerization in EFHD1-overexpressed cells, compared with the control (Figure 3G). Then we knocked down EFHD1 in ccRCC cells (Figure 3H). Transwell assays indicated that silencing of EFHD1 promoted the migration and invasion of ccRCC cells (Figure 3I). In addition, we used a tail vein injection metastasis model to determine whether EFHD1 could suppress the metastasis of ccRCC in vivo. As shown by Figure 3J, the bioluminescence signal was much weaker in mice with injection of EFHD1-overexpressing

ACHN cells. Histologic analyses revealed significantly fewer and smaller metastatic foci in the harvested lung tissues of mice injected with ACHN cells with EFHD1 overexpression (Figure 3K). Together, these findings provide convincing evidence that EFHD1 functions as a suppressor of tumor metastasis in ccRCC.

3.4 | EFHD1 interacts with calcium transporter MCU

Coimmunoprecipitation-MS was used to screen the proteins binding to EFHD1. Proteins immunoprecipitated by EFHD1 Ab or control IgG were collected, separated by SDS-PAGE, and silver-stained to visualize (Figure 4A). Mass spectrometry was then utilized for the screening of EFHD1-interacting proteins. A total of 47 candidates were identified (Figure 4B). The interacting network of the 47 proteins was constructed (Figure 4C). We further analyzed the intracellular localization of the 47 proteins at the UniProt website (http://www.uniprot.org/), and found that 15 proteins localized in the mitochondria (Figure 4D). As EFDH1 was previously identified as a calcium ion-regulating protein, the core mitochondrial calcium ion transporter MCU was chosen for further investigation. We found that EFHD1 and MCU were similarly enriched in mitochondria (Figure 4E). Coimmunoprecipitation experiments were undertaken to verify the binding of EFHD1-Flag and MCU-HA. The results showed that MCU-HA was co-immunoprecipitated by EFHD1-Flag (Figure 4F), and EFHD1-Flag could be found in the immunoprecipitant mediated by MCU-HA (Figure 4G). We next determined the specific domain of EFHD1 for the interaction with MCU. According to the structure of EFHD1, we generated three EFHD1 truncated constructs fused to Flag (Figure 4H). Results of coimmunoprecipitation experiments indicated that the 1–90 amino acids of EFHD1 protein retained the ability of binding MCU, suggesting that EFHD1 interacts with MCU through its N-terminal domain (Figure 4I). We next intended to determine whether the interaction between EFHD1 and MCU affected the mitochondrial Ca^{2+} flow and cell migration in ccRCC. The uptake of mitochondrial Ca^{2+} was markedly enhanced by overexpression of MCU. However, ectopic expression of EFHD1 in MCU-expressing ccRCC cells resulted in a reduction of Ca^{2+} transportation into the mitochondria (Figure 4J,K). Additionally, MCU dramatically promoted ccRCC cell migration and invasion, which was partly abrogated by the overexpression of EFHD1 (Figure 4L). These findings indicate that EFHD1 functions as a metastatic suppressor partly through the blockage of the MCU-mediated Ca^{2+} flow in mitochondria.

3.5 | EFHD1 suppresses tumor metastasis through the STARD13/YAP pathway in ccRCC

To further reveal the mechanism of EFHD1-induced suppression of ccRCC metastasis, we used DIA-based MS to present the differentially expressed proteins in response to EFHD1 overexpression in ACHN and 769-P cells. The results of the PLGEM algorithm showed that the mean and SD of the quantitative protein values were linearly correlated after normalization, with correlation coefficients of 0.988 and 0.994, respectively. The Q-Q plot test revealed that the distribution of residuals tended to be normally distributed, indicating a good fit of PLGEM and good reproducibility of the data (Figure 5A,B). According to the PLGEM algorithm, we obtained 21 proteins that were upregulated (p-value <0.05, fold change ≥1.5) in EFHD1-overexpressed cells (Figure 5C). A heatmap shows the alteration of these 21 proteins (Figure 5D). In addition, KEGG analyses indicated that the Hippo pathway was enriched in EFHD1-overexpressing cells by RNA-seq (Figure 5E). Hippo-YAP signaling promotes growth and metastasis in human cancers.[21] STARD13 was able to enhance the phosphorylation of YAP at Ser127 to consequently suppress its nucleus translocation and the activation of Hippo-YAP signaling.[22,23] STARD13 was upregulated by EFHD1 in our DIA-based MS data, and was therefore chosen for further investigation. Significant increases of STARD13 protein expression and phosphorylated YAP at Ser127 were observed in ccRCC cells with EFHD1 overexpression (Figure 5F). Subcellular fractionation experiments showed that the nuclear YAP was decreased upon EFHD1 overexpression (Figure 5G). Rescued experiments demonstrated that knockdown of STARD13 markedly reduced the phosphorylation of YAP at Ser127 enhanced by EFHD1 (Figure 5H). These data suggest that EFHD1 upregulates STARD13 to inhibit YAP translocation into nucleus, and to consequently inhibit the activation of the YAP pathway in ccRCC.

To determine whether EFHD1 exerted its tumor suppressor activity by modulating the STARD13/YAP pathway, we undertook rescue experiments by overexpressing EFHD1 in cells with or without STARD13 knockdown. Transwell assays showed that the knockdown of STARD13 reversed the suppressive effect of EFHD1 overexpression on cell migration and invasion (Figure 5I). Similar to the effect of STARD13 silence, overexpression of MCU could inhibit the upregulation of STARD13 and phosphorylation of YAP at Ser127 in ACHN and 769-P cells with EFHD1 overexpression (Figure 5J). Taken together, our data indicate that EFHD1 shows antitumor activity through the interaction of MCU to modulate STARD13/YAP signaling in ccRCC.

4 | DISCUSSION

Plenty of studies have shown that mitochondrial dysfunction is essential to trigger tumor metastasis.[24,25] However, the biological functions and the underlying mechanisms of a serial of mitochondrial proteins have not been well investigated. The present study screened 30 differentially expressed mitochondrial proteins through the TCGA-KIRC and CPTAC cohorts. A seven-gene signature that is of prognostic implication was generated by univariate Cox analysis and LASSO analysis. Further investigations revealed the tumor suppressor role of EFHD1, a member of the seven-gene signature, in the progression of ccRCC through MCU/STARD13/YAP signaling (Figure 6). Our study revealed the function and the mechanism of an understudied protein, EFHD1, and provided new insight into the clinical strategy of cancer management.

Calcium ions are second messengers in cells, and play an important role in regulating cell functions. Mitochondria act as substantial

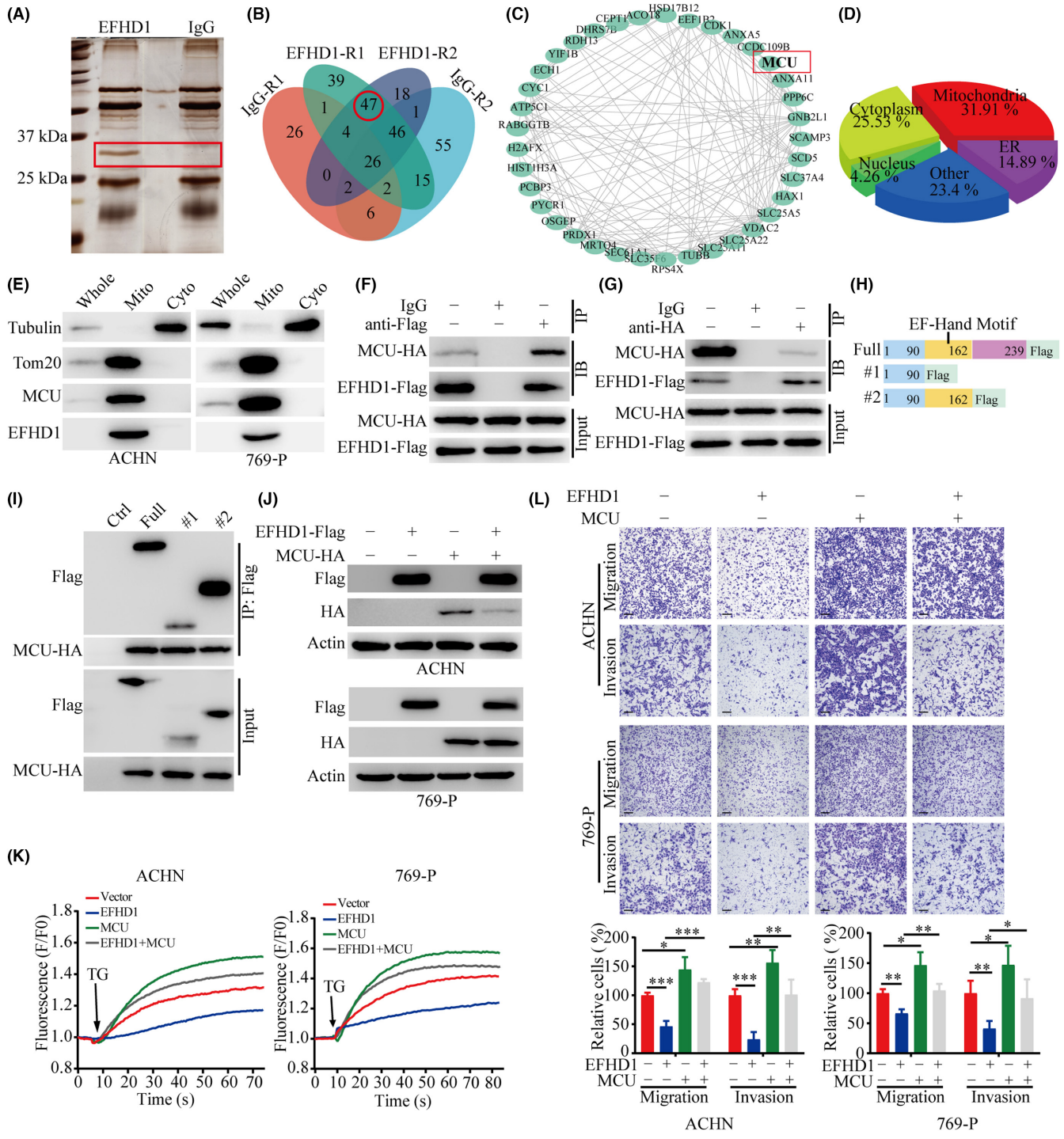

FIGURE 4 EFHD1 interacts with calcium transporter mitochondrial calcium uniporter (MCU). (A). Proteins that interacted with EFHD1 were silver-stained and identified by coimmunoprecipitation–mass spectrometry. (B) Venn diagram showing a total of 47 candidates that interacted with EFHD1, identified by overlapping two independent screenings. (C) Interacting network of EFHD1 was constructed, and mitochondrial function was enrichment. (D) Pie chart shows intracellular localization of the EFHD1 interacting protein. (E) EFHD1 and MCU were enriched in mitochondrial components. (F) EFHD1-Flag and MCU-HA plasmids were transfected into 293T cells, EFHD1-Flag was coimmunoprecipitated by anti-Flag Ab, and MCU-HA was detected. (G) EFHD1-Flag and MCU-HA plasmids were transfected into 293T cells, MCU-HA was coimmunoprecipitated by anti-HA Ab, and EFHD1-Flag was detected. (H) Diagram of EFHD1 WT and mutation constructs with the different domains. (I) The indicated EFHD1-Flag plasmid transfected into 293T cells, and EFHD1-Flag and MCU-HA complexes were coimmunoprecipitated by anti-Flag Ab, and MCU-HA was detected. (J) EFHD1 and MCU were overexpressed in ACHN and 769-P cells. (K) Overexpressed MCU-HA rescued the suppression of mitochondrial calcium ion uptake induced by EFHD1 in ACHN and 769-P cells. (L) Overexpressed MCU-HA rescued the suppression of migration and invasion induced by EFHD1 in ACHN and 769-P cells. $^{*}p < 0.05$, $^{**}p < 0.01$, $^{***}p < 0.001$ (one-way ANOVA). Scale bar, 300 μm. ER, endoplasmic reticulum; IB, immunoblotting; TG, thapsigargin.

intracellular calcium ion containers to mediate calcium ion balance in the cytoplasm. Mitochondrial Ca^{2+} regulates several mitochondrial functions, from metabolism to apoptosis.[26–29] Alterations in mitochondrial Ca^{2+} fluxes influence malignant transformation and tumor progression.[30–32] Mitochondrial Ca^{2+} transport is strictly regulated; MCU and its regulatory proteins are the core calcium transporter of mitochondria.[33,34] Levels of MCU in malignant cells positively correlate with mitochondrial Ca^{2+} uptake, ROS production, and propensity for metastatic dissemination.[35,36] EFHD1 is a 27 kDa mitochondrial protein consisting of two Ca^{2+}-binding EF-hand domains to regulate mitochondrial metabolism at the interface between ROS and calcium.[37] We found that EFHD1 directly interacted with MCU, and EFHD1 inhibits mitochondrial Ca^{2+} uptake by blocking MCU. In the present study, we found that EFHD1 was downregulated

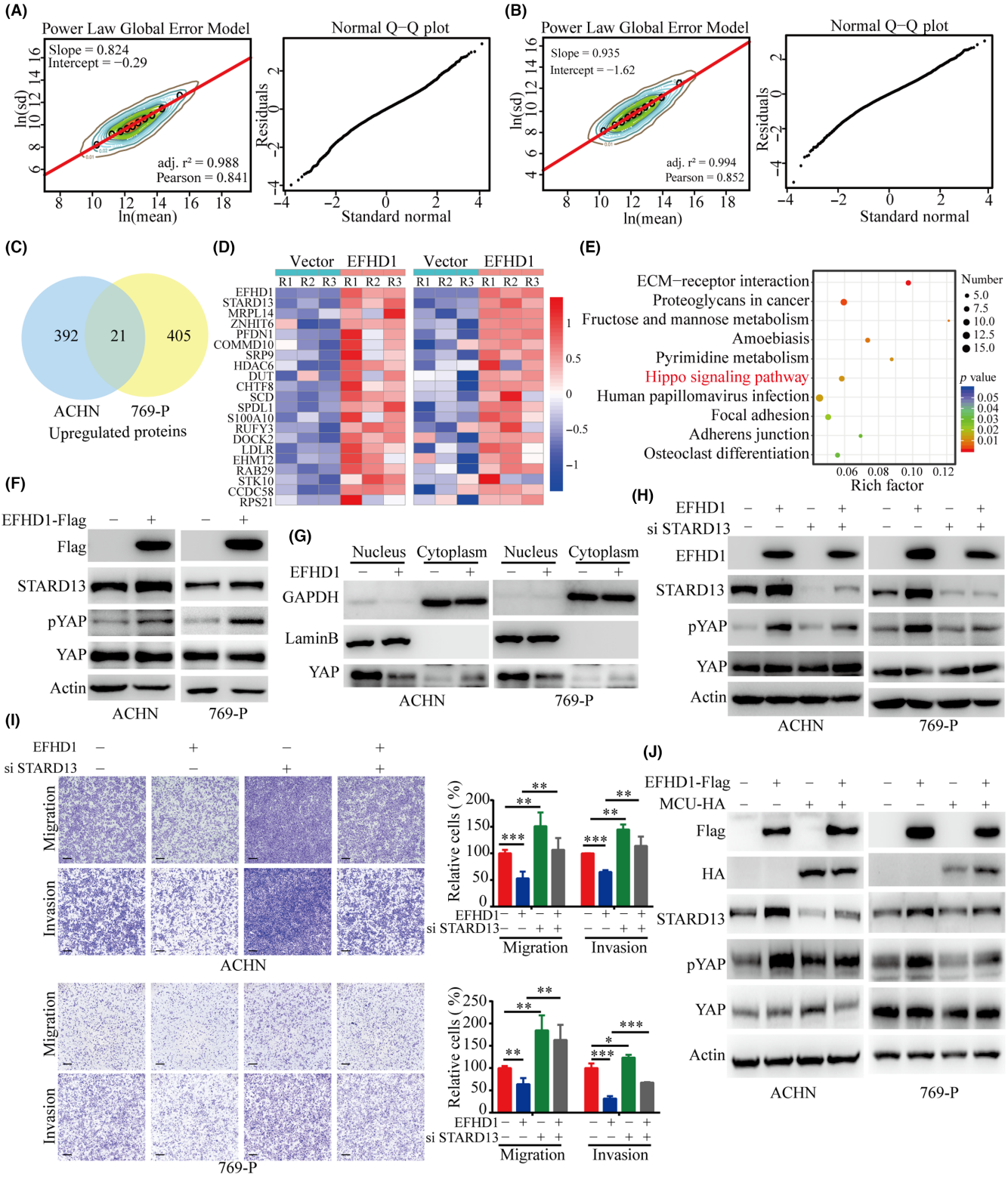

FIGURE 5 EFHD1 suppresses tumor metastasis through the STARD13/YAP pathway in clear cell renal cell carcinoma (ccRCC). (A,B) Power Law Global Error Model was applied to analyze the differences in protein expression in response to EFHD1 overexpression in (A) ACHN and (B) 769-P cells identified by mass spectrometry. (C) Venn diagram showing the intersection of upregulated proteins on EFHD1 overexpressed in ACHN and 769-P cells. (D) A heatmap was drawn to demonstrate the co-upregulated proteins in three independent biological replicates of two ccRCC cell lines. (E) Kyoto Encyclopedia of Genes and Genomes analyses indicated that the Hippo signaling pathway was enriched in ccRCC cells overexpressing EFHD1 by RNA sequencing. (F) Overexpression of EFHD1 increases the protein level of STARD13 and phosphorylated YAP at Ser127. (G) Cellular fragmentation experiments showed that nuclear YAP was decreased but cytosolic YAP was increased in EFHD1-expressing ACHN and 769-P cells. (H). Knockdown of STARD13 reduced the phosphorylation of YAP at Ser127 enhanced by EFHD1 overexpression. (I) Transwell experiments showed that knockdown of STARD13 can rescue the suppressive effect of migration and invasion induced by overexpressed EFHD1. $^{*}p<0.05$, $^{**}p<0.01$, $^{***}p<0.001$ (one-way ANOVA). Scale bar, 300 μm. (J) Overexpressed MCU inhibits the upregulation of STARD13 and phosphorylation of YAP at Ser127 in ACHN and 769-P cells with EFHD1 overexpression.

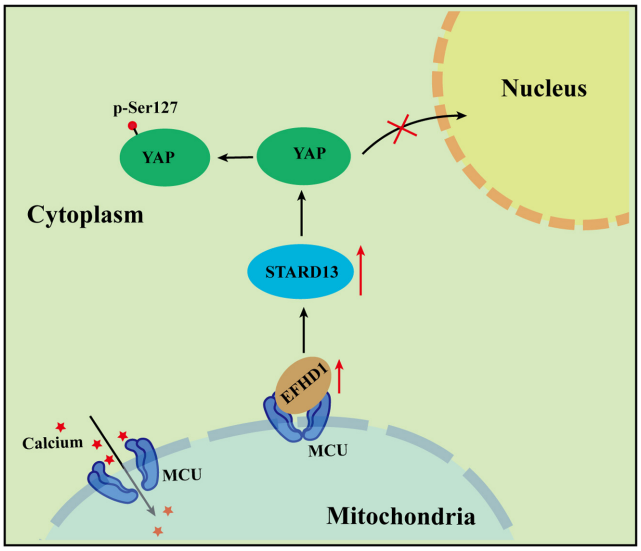

FIGURE 6 Hypothetical model. EFHD1 interacting with MCU coregulates mitochondrial Ca^{2+} uptake, which regulates the STARD13/YAP pathway and ultimately inhibits clear cell renal cell carcinoma metastasis.

in ccRCC tissues at both mRNA and protein levels. Decreased expression of EFHD1 serves as promising prognostic factor in ccRCC. Previous studies have reported that EFHD1 expression was regulated by transcriptional factor HNF4A in HEK293 cells, and promoter methylation in colorectal cancer. Further investigations were required to reveal the molecular mechanism through which EFHD1 was upregulated in ccRCC cells.

STARD13 is one of the RhoGTPase family and is involved in various physiological processes, such as embryogenesis and regulation of microtubule growth. Furthermore, STARD13 acts as a tumor suppressor in many tumors.[38–40] STARD13 can inhibit YAP/TAZ accumulation and transcriptional activity in the nucleus.[22,23] YAP/TAZ, an important responding factor of the Hippo pathway, is hyperactivated in various cancers.[41–44] YAP phosphorylation at Ser127 results in cytosolic retention of YAP protein to inhibit the proliferation, migration, and invasion of various tumors.[45] In our study, we found that EFHD1 upregulated the protein expression of STARD13 and enhanced the phosphorylation of YAP at Ser127 to inhibit the metastasis of ccRCC.

In conclusion, a reliable risk score model of mitochondrial proteins was established to predict ccRCC prognosis in our study. We verified the ability of EFHD1 to inhibit ccRCC cell migration and invasion in vivo. Moreover, we elucidated that EFHD1 exerted antimetastatic activity through interaction of MCU and STARD13 to modulate mitochondrial Ca^{2+} uptake and YAP signaling.

AUTHOR CONTRIBUTIONS

Qing-Yu He, Chris Zhiyi Zhang, and Kun Meng designed experiments, analyzed the data, and wrote the manuscript. Kun Meng and Yuyu Hu performed the experiments and Dingkang Wang, Yuying Li, Fujin Shi, and Jiangli Lu were involved in experimentation and data analysis. Yang Wang and Yun Cao advised on experimental design.

ACKNOWLEDGMENTS

This work was supported by the National Key Research and Development Program of China (2020YFE0202200, 2017YFA0505100), the National Natural Science Foundation of China (31770888, 31570828), and the Guangdong Basic and Applied Basic Research Foundation (2022A1515111106).

CONFLICT OF INTEREST STATEMENT

The authors have no conflict of interest. None of the authors of this manuscript is a current Editor or Editorial Board member of *Cancer Science*.

ETHICS STATEMENT

Approval of the research protocol by an institutional review board: This study was approved by the institutional research ethics committee of Sun Yat-sen University Cancer Center.

Informed consent: N/A.

Registry and registration no. of the study/trial: N/A.

Animal studies: Animal studies were approved by the Ethics Committee for Animal Experiments of Jinan University (IACUC-20211109-06).

ORCID

Kun Meng https://orcid.org/0000-0003-4478-2553

REFERENCES

1. Kustatscher G, Collins T, Gingras AC, et al. An open invitation to the understudied proteins initiative. *Nat Biotechnol*. 2022;40:815-817.
2. Hsieh JJ, Purdue MP, Signoretti S, et al. Renal cell carcinoma. *Nat Rev Dis Primers*. 2017;3:17009.
3. Jonasch E, Gao J, Rathmell WK. Renal cell carcinoma. *BMJ*. 2014;349:g4797.
4. Galvan DL, Green NH, Danesh FR. The hallmarks of mitochondrial dysfunction in chronic kidney disease. *Kidney Int*. 2017;92:1051-1057.

5. Zaravinos A, Deltas C. ccRCC is fundamentally a metabolic disorder. *Cell Cycle*. 2014;13:2481-2482.
6. Linehan WM, Schmidt LS, Crooks DR, et al. The metabolic basis of kidney cancer. *Cancer Discov*. 2019;9:1006-1021.
7. Du W, Zhang L, Brett-Morris A, et al. HIF drives lipid deposition and cancer in ccRCC via repression of fatty acid metabolism. *Nat Commun*. 2017;8:1769.
8. Yuan Y, Ju YS, Kim Y, et al. Comprehensive molecular characterization of mitochondrial genomes in human cancers. *Nat Genet*. 2020;52:342-352.
9. Weinberg SE, Chandel NS. Targeting mitochondria metabolism for cancer therapy. *Nat Chem Biol*. 2015;11:9-15.
10. Porporato PE, Filigheddu N, Pedro JMB, Kroemer G, Galluzzi L. Mitochondrial metabolism and cancer. *Cell Res*. 2018;28:265-280.
11. Ulisse V, Dey S, Rothbard DE, et al. Regulation of axonal morphogenesis by the mitochondrial protein Efhd1. *Life Sci Alliance*. 2020;3:e202000753.
12. Eberhardt DR, Lee SH, Yin X, et al. EFHD1 ablation inhibits cardiac mitoflash activation and protects cardiomyocytes from ischemia. *J Mol Cell Cardiol*. 2022;167:1-14.
13. Dutting S, Brachs S, Mielenz D. Fraternal twins: Swiprosin-1/EFhd2 and Swiprosin-2/EFhd1, two homologous EF-hand containing calcium binding adaptor proteins with distinct functions. *Cell Commun Signal*. 2011;9:2.
14. Takane K, Midorikawa Y, Yagi K, et al. Aberrant promoter methylation of PPP1R3C and EFHD1 in plasma of colorectal cancer patients. *Cancer Med*. 2014;3:1235-1245.
15. Huang H, Zhu L, Huang C, et al. Identification of hub genes associated with clear cell renal cell carcinoma by integrated bioinformatics analysis. *Front Oncol*. 2021;11:726655.
16. Davidson B, Stavnes HT, Risberg B, et al. Gene expression signatures differentiate adenocarcinoma of lung and breast origin in effusions. *Hum Pathol*. 2012;43:684-694.
17. Grigo K, Wirsing A, Lucas B, Klein-Hitpass L, Ryffel GU. HNF4 alpha orchestrates a set of 14 genes to down-regulate cell proliferation in kidney cells. *Biol Chem*. 2008;389:179-187.
18. Lucas B, Grigo K, Erdmann S, Lausen J, Klein-Hitpass L, Ryffel GU. HNF4alpha reduces proliferation of kidney cells and affects genes deregulated in renal cell carcinoma. *Oncogene*. 2005;24:6418-6431.
19. Meng K, Lu S, Yan X, et al. Quantitative mitochondrial proteomics reveals ANXA7 as a crucial factor in mitophagy. *J Proteome Res*. 2020;19:1275-1284.
20. Wang Y, Zhang J, Li YJ, et al. MEST promotes lung cancer invasion and metastasis by interacting with VCP to activate NF-kappaB signaling. *J Exp Clin Cancer Res*. 2021;40:301.
21. Moya IM, Halder G. Hippo-YAP/TAZ signalling in organ regeneration and regenerative medicine. *Nat Rev Mol Cell Biol*. 2019;20:211-226.
22. Jin X, Yu W, Ye P. MiR-125b enhances doxorubicin-induced cardiotoxicity by suppressing the nucleus-cytoplasmic translocation of YAP via targeting STARD13. *Environ Toxicol*. 2022;37:730-740.
23. Zheng L, Xiang C, Li X, et al. STARD13-Correlated ceRNA network-directed inhibition on YAP/TAZ activity suppresses stemness of breast cancer via co-regulating hippo and rho-GTPase/F-Actin signaling. *J Hematol Oncol*. 2018;11:72.
24. Zong WX, Rabinowitz JD, White E. Mitochondria and cancer. *Mol Cell*. 2016;61:667-676.
25. Wallace DC. Mitochondria and cancer. *Nat Rev Cancer*. 2012;12:685-698.
26. Garbincius JF, Elrod JW. Mitochondrial calcium exchange in physiology and disease. *Physiol Rev*. 2022;102:893-992.
27. Calvo-Rodriguez M, Bacskai BJ. Mitochondria and calcium in Alzheimer's disease: from cell signaling to neuronal cell death. *Trends Neurosci*. 2021;44:136-151.
28. Wang N, Yin J, You N, et al. TWIST1 preserves hematopoietic stem cell function via the CACNA1B/Ca2+/mitochondria axis. *Blood*. 2021;137:2907-2919.
29. Pathak T, Trebak M. Mitochondrial Ca(2+) signaling. *Pharmacol Ther*. 2018;192:112-123.
30. Marchi S, Giorgi C, Galluzzi L, Pinton P. Ca(2+) fluxes and cancer. *Mol Cell*. 2020;78:1055-1069.
31. Wang X, Li Y, Li Z, et al. Mitochondrial calcium uniporter drives metastasis and confers a targetable cystine dependency in pancreatic cancer. *Cancer Res*. 2022;82:2254-2268.
32. Lombardi AA, Gibb AA, Arif E, et al. Mitochondrial calcium exchange links metabolism with the epigenome to control cellular differentiation. *Nat Commun*. 2019;10:4509.
33. Fan M, Zhang J, Tsai CW, et al. Structure and mechanism of the mitochondrial Ca(2+) uniporter holocomplex. *Nature*. 2020;582:129-133.
34. Williams GS, Boyman L, Chikando AC, Khairallah RJ, Lederer WJ. Mitochondrial calcium uptake. *Proc Natl Acad Sci U S A*. 2013;110:10479-10486.
35. Wang P, Xu S, Xu J, et al. Elevated MCU expression by CaMKIIdeltaB limits pathological cardiac remodeling. *Circulation*. 2022;145:1067-1083.
36. Zhao H, Li T, Wang K, et al. AMPK-mediated activation of MCU stimulates mitochondrial Ca(2+) entry to promote mitotic progression. *Nat Cell Biol*. 2019;21:476-486.
37. Hou T, Jian C, Xu J, et al. Identification of EFHD1 as a novel Ca(2+) sensor for mitoflash activation. *Cell Calcium*. 2016;59:262-270.
38. Abdellatef S, Fakhoury I, Haddad MA, et al. StarD13 negatively regulates invadopodia formation and invasion in high-grade serous (HGS) ovarian adenocarcinoma cells by inhibiting Cdc42. *Eur J Cell Biol*. 2022;101:151197.
39. Naumann H, Rathjen T, Poy MN, Spagnoli FM. The RhoGAP Stard13 controls insulin secretion through F-Actin remodeling. *Mol Metab*. 2018;8:96-105.
40. Al Haddad M, El-Rif R, Hanna S, et al. Differential regulation of rho GTPases during lung adenocarcinoma migration and invasion reveals a novel role of the tumor suppressor StarD13 in invadopodia regulation. *Cell Commun Signal*. 2020;18:144.
41. Nguyen CDK, Yi C. YAP/TAZ signaling and resistance to cancer therapy. *Trends Cancer*. 2019;5:283-296.
42. Shen Y, Wang X, Liu Y, et al. STAT3-YAP/TAZ signaling in endothelial cells promotes tumor angiogenesis. *Sci Signal*. 2021;14:eabj8393.
43. Zhu H, Yan F, Yuan T, et al. USP10 promotes proliferation of hepatocellular carcinoma by deubiquitinating and stabilizing YAP/TAZ. *Cancer Res*. 2020;80:2204-2216.
44. Zanconato F, Forcato M, Battilana G, et al. Genome-wide association between YAP/TAZ/TEAD and AP-1 at enhancers drives oncogenic growth. *Nat Cell Biol*. 2015;17:1218-1227.
45. Moroishi T, Hansen CG, Guan KL. The emerging roles of YAP and TAZ in cancer. *Nat Rev Cancer*. 2015;15:73-79.

SUPPORTING INFORMATION

Additional supporting information can be found online in the Supporting Information section at the end of this article.

How to cite this article: Meng K, Hu Y, Wang D, et al. EFHD1, a novel mitochondrial regulator of tumor metastasis in clear cell renal cell carcinoma. *Cancer Sci*. 2023;114:2029-2040. doi:10.1111/cas.15749